Atomically resolved STM images of carbon nanotube defects produced by Ar^+ irradiation

Z. Osváth, G. Vértesy, L. Tapasztó, F. Wéber, Z. E. Horváth, J. Gyulai, and L. P. Biró
Research Institute for Technical Physics and Materials Science, H-1525 Budapest, P.O. Box 49, Hungary
(Received 11 February 2005; published 14 July 2005)

Multiwall carbon nanotubes (MWCNTs) dispersed on graphite on highly oriented pyrolytic graphite (HOPG) substrate were irradiated with Ar^+ ions of 30 keV. The irradiated samples were investigated by scanning tunneling microscopy (STM) and spectroscopy (STS) in air. The irradiation-induced defects appear as hillocklike protrusions on the nanotube walls, similar to the hillocks observed earlier on ion irradiated HOPG. The results are in agreement with recent predictions, which attribute the STM features produced by ion irradiation to local modifications of the electronic structure. "$\sqrt{3}\times\sqrt{3}R$" type superstructures are also observed near some of the defects. After annealing at 450 °C in nitrogen atmosphere, the irradiated MWCNTs were investigated again by STM. The effect of heat treatment on the irradiation-induced nanotube defects is also discussed.

DOI: 10.1103/PhysRevB.72.045429 PACS number(s): 73.22.−f, 07.79.Cz

I. INTRODUCTION

Carbon nanotubes (CNTs) usually are regarded as perfect tubes made from sheets of graphite, which are rolled into cylinders.[1] However, defects like vacancies, vacancy-related defects or nonhexagonal carbon rings may occur in the structure of nanotubes. The specific combination of such defects may lead to the formation of nanotube junctions,[2,3] branched nanotubes,[4,5] or regularily coiled carbon nanotubes.[6–9] It has been shown that defects also influence the transport properties of the nanotubes.[10] Topological defects may occur in the as-grown nanotubes, or they can be generated by several methods like chemical treatment or irradiation with charged particles. Recent experiments show that both electron and heavy ion irradiation can modify the structure and dimensions of CNTs.[11–14] Irradiation with heavy ions may induce interesting phenomena like welding,[15,16] crosslinking,[17,18] or coalescence[19] of the nanotubes. *In situ* X-ray photoelectron spectroscopy (XPS) and Auger electron spectroscopy (AES) analysis[20] showed that irradiation with Ar^+ ions produces dangling bonds (vacancies) on the surface of nanotubes and may cause shrinkage of the nanotube diameters. Ar^+ irradiation was used in order to create tunneling barriers in multiwall carbon nanotubes,[21] and also to control the shape of the nanotubes.[22] Furthermore, Ni *et al.*[23] used CF_3^+ ion beams to functionalize nanotubes, since defects are supposed to be the preferred sites for chemical reactions.[24] Other groups have investigated the possibility of using CNTs as masks during irradiation, in order to produce ultranarrow metal nanowires.[25,26] A brief overview on the irradiation-induced effects in carbon nanotubes has been given recently.[27] Krasheninnikov and co-workers[28,29] employed the tight-binding technique to calculate scanning tunneling microscopy (STM) images of individual vacancies created by irradiation. They have calculated also the STM images of other vacancy-related defects, and have demonstrated that different type of defects have different signatures in the STM images.[30] The STM signatures of native topological defects (nonhexagonal carbon rings) were also simulated.[31,32] Recent experimental and theoretical STM and scanning tunneling spectroscopy (STS) analysis revealed a pentagon-heptagon pair at a particular nanotube junction.[33] Such defects were created also in single graphene layers and examined by high-resolution transmission electron microscopy (HR-TEM).[34]

STM is a very effective tool to detect atomic-scale defects in the walls of CNTs. In this work we present the results from experimental STM investigation of irradiated multiwall CNTs (MWCNTs).

II. EXPERIMENTAL DETAILS

The multiwalled carbon nanotubes used in this study were produced using the electric arc-discharge technique employing two graphite electrodes. The growth was carried out in helium atmosphere (66 kPa) by applying a current of 100 A and a voltage of 25 V. After a typical experimental time of 7 min, about 80 wt % of the evaporated material resulted in the formation of a cylindrical deposit grown onto the graphite cathode and whose inner black core contained the MWCNTs.

1 mg of nanotube-sample was ultrasonicated in toluene for 60 min, and droplets of the suspension were dispersed on graphite on highly oriented pyrolytic graphite (HOPG) substrate. After the evaporation of toluene, the supported nanotubes were irradiated with Ar^+ ions of 30 keV, with a dose of $D=5\times10^{11}$ ion/cm^2. The low dose of ions was chosen in order to produce individual defects in the nanotube walls. Without further manipulation, the irradiated MWCNTs were investigated with STM and STS under ambient conditions. The STM measurements were carried out in constant current mode with tunneling currents of 0.3–1 nA and bias voltages in the range of 0.1–0.5 V. Atomic resolution images were typically achieved with the current set to 1 nA and 0.1 V bias. The STM tips were prepared by mechanically cutting from a Pt/Ir wire.

III. RESULTS AND DISCUSSION

The STM observation of irradiated multiwall CNTs revealed the signatures of the defects induced by the Ar^+ ions.

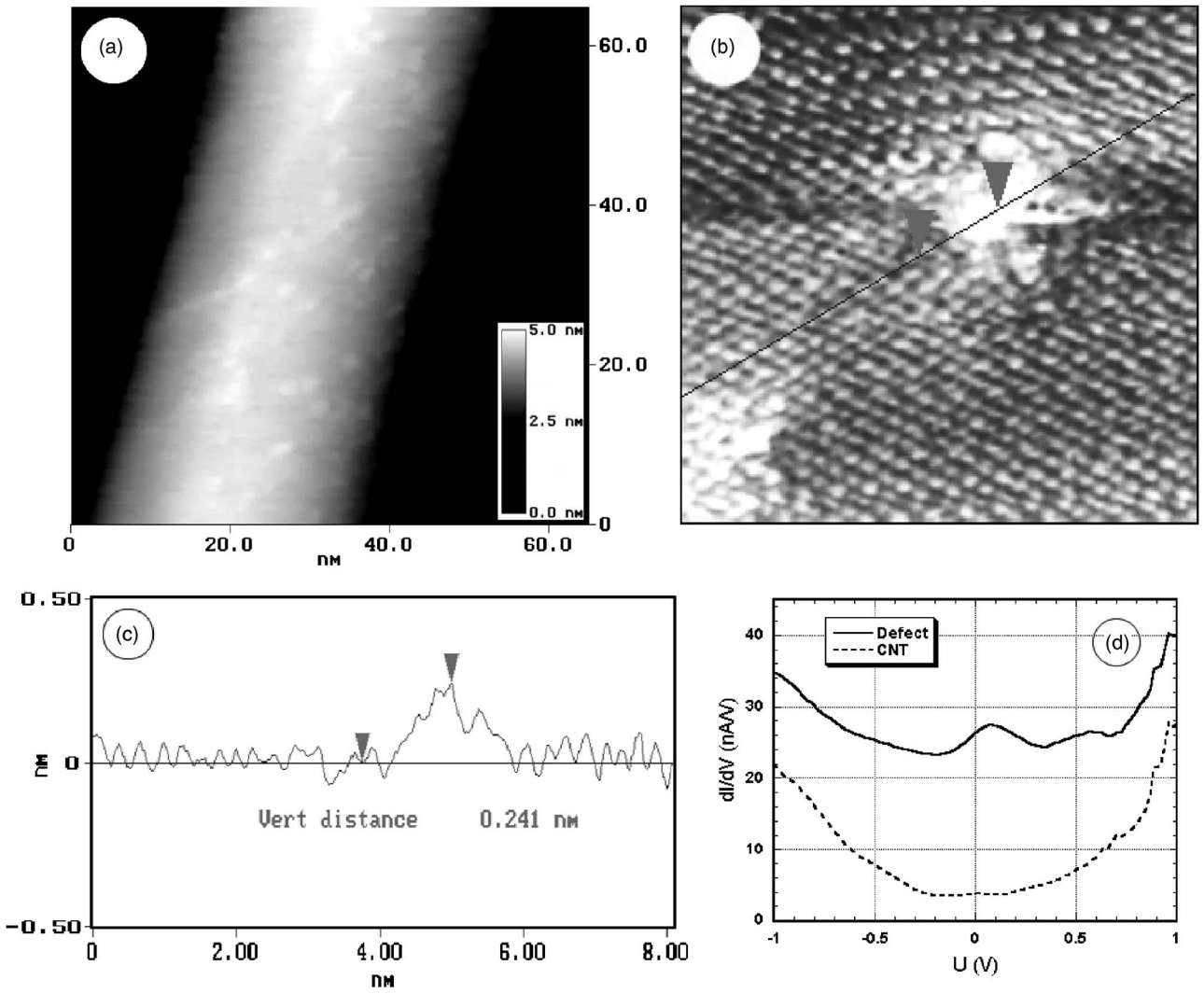

FIG. 1. (a) MWCNT with defects (hillocklike protrusions) created by irradiation. (b) Atomic resolution STM image of a nanotube defect. (c) Cross-sectional line showing the apparent height of the defect. (d) dI/dV curves recorded above the defect presented in (b) (continuous line), and above a defect-free region of the CNT (dashed line).

These defects appear as protrusions (tunneling-current maxima) in the STM images, which is in agreement with theoretical predictions.[28,29] Figure 1(a) depicts a portion of an irradiated multiwall CNT, containing around 30 defects (no defects could be detected on the original sample). These protrusions are similar to the hillocks observed earlier on irradiated HOPG surface.[35,36] An atomic resolution STM image of a nanotube-defect is presented in Fig. 1(b). The cross-sectional line shows that the apparent height of the hillock is around 0.24 ± 0.03 nm [Fig. 1(c)]. One can observe that atomic resolution is lost at the hillock, and one cannot directly determine which type of defect is (vacancy, nonhexagonal ring, etc.).

Above the defect shown in Fig. 1(b) we performed also STS measurements. The dI/dV curves are plotted in Fig. 1(d), where the dashed line corresponds to the curve measured at a relatively large distance from the defect, i.e., above a defect-free region. It is obvious from the figure that an additional peak appears in the local density of states (LDOS) at 0.1 eV above the Fermi energy. These additional electronic states contribute to the tunneling process and as a result the tunneling current increases as compared with the defect free region when the STM tip reaches the defect site during scaning. Thus the STM tip has to move upwards on the z axis (farther from the nanotube surface) in order to keep constant the value of the tunneling current set previously in the microscope (constant current operating mode). This vertical movement of the tip produces the "heights" observed at the defect sites in the topographic images. This result is in agreement with calculations which show that both vacancies[28,37] and nonhexagonal carbon rings[31,32] may act as local perturbations and can change the LDOS features near the Fermi level.

It is well known from the literature, that carbon nanotube defects (introduced for example during chemical purification) can be removed by annealing the samples at high temperatures.[38] In order to monitor with STM the effect of elevated temperature on the defects induced by irradiation, we annealed the irradiated nanotube sample at 450 °C for 90 min. The heating was done under a nitrogen atmosphere

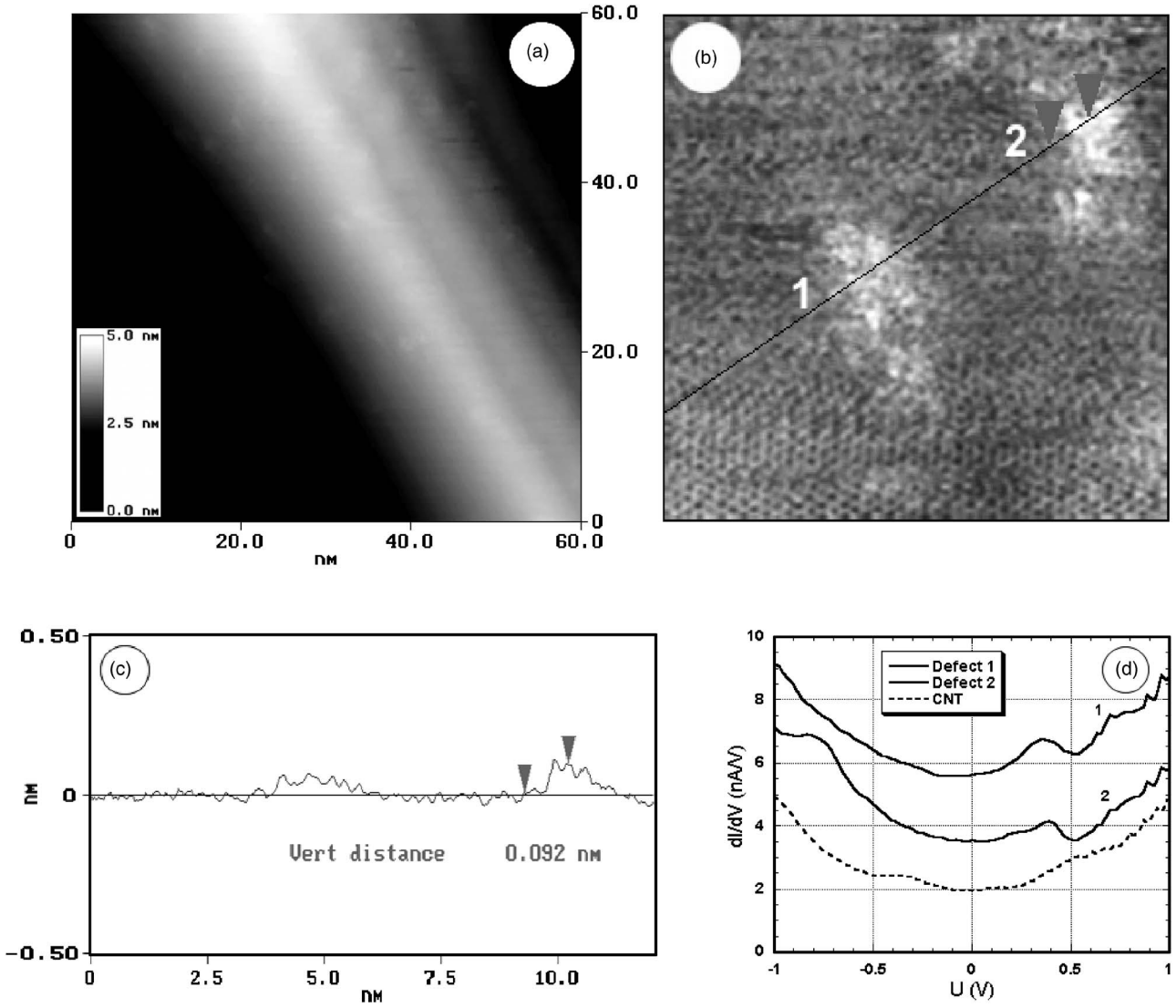

FIG. 2. (a) Irradiated MWCNT with defects, after heat treatment. (b) STM image of two nanotube defects. (c) Cross-sectional line showing the apparent heights of the two defects. (d) dI/dV curves recorded above the two defects presented in (b) (continuous lines), and above a defect-free region of the CNT (dashed line).

of 5 bars. After annealing, the sample was investigated again with STM under ambient conditions. Figure 2(a) shows a portion of a multiwall CNT after the heat treatment. One can see that—using the same tunneling conditions—the irradiation-induced hillocks are not very well observed, compared to the case before annealing [Fig. 1(a)]. However, when scanning a smaller area (12×12 nm^2), the defect sites can be distinguished again. Figure 2(b) shows two defect sites labeled 1 and 2. The apparent heights of these hillocks turned out to be less than 0.1 ± 0.03 nm [see the cross-sectional line in Fig. 2(c)], which is much lower than the 0.24 ± 0.03 nm measured before heating the sample [Fig. 1(c)]. This result nicely shows how CNT defects tend to heal already at moderate temperatures.

We performed STS measurements at the two defect sites presented in Fig. 2(b). The additional peaks above the Fermi energy are observed on both curves [Fig. 2(d)]. However, in this case the peaks are at 0.35 eV above the Fermi energy, i.e., at energies higher with around 0.25 eV than before heating. This observation indicates that the nature of the defects changes during the annealing, these defects produce donor-like surface states. Such kind of states can appear assuming that nitrogen adsorbs at the defect sites.[39,40] Another possible mechanism is the transformation of the vacancy-type defects, during the annealing process, into nonhexagonal ring-type defects by dangling bond saturation, predicted by molecular dynamical simulations.[30]

In Fig. 3 we show an atomic resolution STM image of a multiwall CNT with defects. The image was recorded after the heat treatment. Several defect sites can be distinguished in the figure, separated by a couple of nanometers from each other. In the close vicinity of these defects we observed periodic oscillations in the LDOS (superstructures). A magnified portion of Fig. 3 is presented in Fig. 4 where the cross-sectional lines show that the period of these oscillations is about 0.39 nm, which is larger than the period of ~0.25 nm indicated by the atomic structure (see the inset). The amplitude of these oscillations decreases with increasing distance,

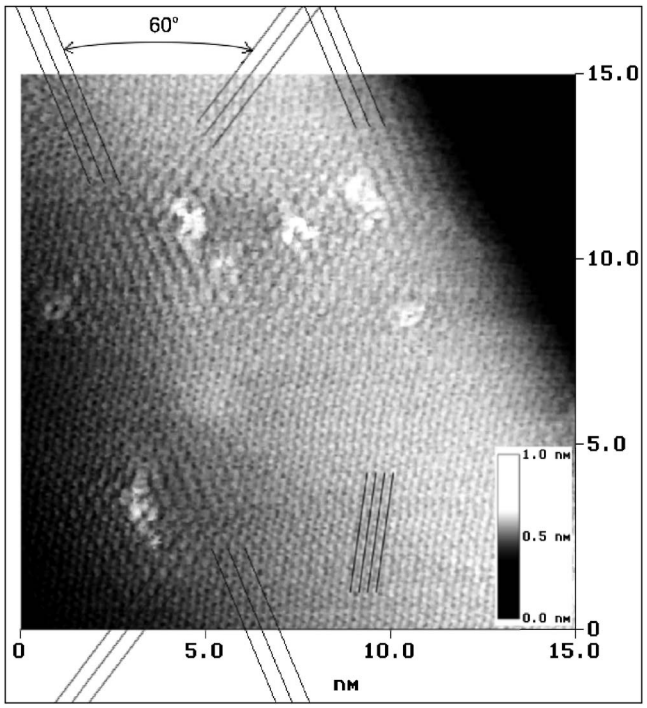

FIG. 3. Atomic resolution STM image of a MWCNT with several defects created by Ar^+ ion irradiation. Electronic superstructures of $\sqrt{3}\times\sqrt{3}R$ type can be observed near some of the defects. The lines due to the increased LDOS have the same orientation within one group, while the groups are oriented at 60°.

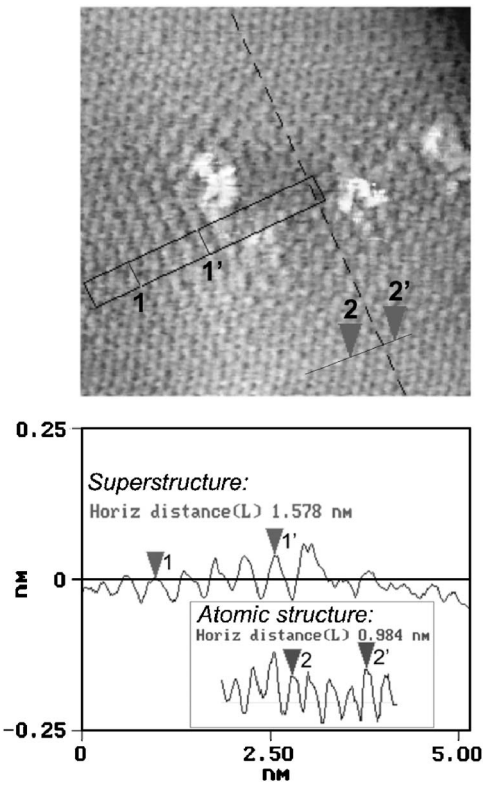

FIG. 4. MWCNT portion magnified from Fig. 3. The cross-sectional lines show the period of the observed superstructures $(1-1')$, and the period determined by the atomic structure $(2-2'$, inset). In both cases the value given as "horizontal distance" corresponds to the distance measured between the two markers.

and it vanishes within a distance of about 3 nm from the defect. These superstructures closely resemble the "$\sqrt{3}\times\sqrt{3}R$" type superstructures observed earlier on HOPG surfaces[36,41] ($R=0.246$ nm is the distance between B-site atoms in the HOPG) and predicted theoretically for single wall CNTs (SWCNTs) with vacancies.[28,37] The experimentally observed patterns can be explained considering the local perturbation of the electronic structure caused by the defect, without taking into consideration any rearrangement in the atomic structure of the MWCNT. The period of the atomic resolution pattern observed in the defect free regions of the MWCNT is ~0.25 nm (Fig. 4), just like in case of HOPG, which shows that the two outermost graphene layers must exhibit an *ABAB* type stacking,[42] i.e., the outermost layer has two nonequivalent atoms. In this case the wave functions at the Fermi energy can be expressed as a symmetric and an antisymmetric linear combination of the allowed wave functions near the Fermi energy.[43] Moreover, in the case of a CNT—specified by the chiral vector $\vec{L}$—the electron wave function is required to satisfy the periodic boundary condition $\Psi(\vec{r})=\Psi(\vec{r}+\vec{L})$, giving rise to a quantization of the $k_\perp$, the wave-vector component perpendicular to the tube axis.[44]

In order to reproduce the experimentally found superstructures, we write the symmetric wave function in form of the sum of cosines, and the antisymmetric wave function as a sum of sinuses, similarly to the wave functions constructed by Shedd and Russell for graphite,[45] but also considering the quantization of the angular momentum component of the wave vector, specific to carbon nanotubes[46]

$$\Psi_S(\vec{r})=\sum_{i=1}^{3} a_i \cos[(\vec{k}_Z^i+\vec{k}_\perp^i)\cdot\vec{r}] \text{ and}$$

$$\Psi_A(\vec{r})=\sum_{i=1}^{3} b_i \sin[(\vec{k}_Z^i+\vec{k}_\perp^i)\cdot\vec{r}], \quad (1)$$

where $\vec{k}^i=(\vec{k}_Z^i+\vec{k}_\perp^i)$ are wave vectors pointing toward the corners of the Brillouin zone, with $\vec{k}_Z^i$ the axial and $\vec{k}_\perp^i$ the circumferential components. The $\vec{k}_\perp$ component has discrete allowed values in case of nanotubes

$$\vec{k}_\perp=\frac{2\pi}{L}\left(n-\frac{\nu}{3}\right), \quad (2)$$

where n is an integer, characterizing the angular momentum component of the electron, L is the tube circumference, and $\nu=0\pm1$.[46] The effect of a localized perturbation can be considered by adding a scattered wave to the symmetric solution.[43] Considering a constructive interference between the normal symmetric wave function and the added scattered wave function,[43,47] the experimentally observed superstructure is well reproduced. A computer generated grey-scale plot of the calculated electron density as a function of position is shown in Fig. 5. The calculated value of the distance between adjacent rows of high LDOS sites (at the Fermi energy) is $(3/2)R=0.37$ nm, which is in a good agreement

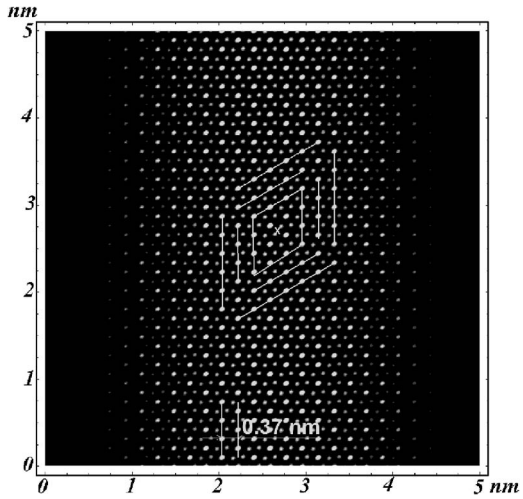

FIG. 5. 2D grey-scale plot of the calculated interference patterns in the electron density of a MWCNT with a "zigzag" type outer shell.

with our experimental findings. Furthermore, the theoretical results show that as long as the chirality of the tube is unchanged, the orientation of the superstructures remains the same. The experimental results are in agreement with this statement, the STM image in Fig. 3 shows that the superstructures surrounding different defects have the same orientation (see the guiding lines in the figure). The angle of 60° between the observed interference patterns is due to the allowed wave propagation directions near the Fermi energy.[45]

IV. CONCLUSIONS

We have investigated irradiated multiwall CNTs by STM and STS. Atomic resolution STM images of the irradiated CNTs were presented, showing the irradiation-induced defects as hillocklike protrusions (tunneling current maxima), corresponding to the locally changed electronic structure at the defect sites. The heights of these protrusions decreased after a heat treatment, indicating the healing tendency of the defects. STS measurements also show that the nature of the defects changed during the annealing. Electronic superstructures of $\sqrt{3}\times\sqrt{3}R$ type (oscillations in the LDOS) were observed near some of the irradiation-induced defects. These experimentally found superstructures could be well reproduced by considering a constructive interference between normal electron wave functions and those scattered by the defect. The measurements show that the superstructures observed on a nanotube with a given chirality have the same orientation.

ACKNOWLEDGMENTS

This work was supported by OTKA Grant Nos. T 43685 and T 43704 in Hungary and the "Nanotechnológia 2-NKFP 3A071_04" grant. The authors thank the Group of Carbonaceous Nanostructures and Nanotechnology at the Intstituto de Carboquímica, Zaragoza (CSIC) for the MWCNT sample and fruitful scientific discussions.

[1] M. S. Dresselhaus, G. Dresselhaus, and P. Avouris, *Carbon Nanotubes, Synthesis, Structure, Properties and Applications* (Springer, Berlin, 2001).
[2] V. Meunier, L. Henrard, and Ph. Lambin, Phys. Rev. B **57**, 2586 (1998).
[3] J. Han, M. P. Anantram, R. L. Jaffe, J. Kong, and H. Dai, Phys. Rev. B **57**, 14983 (1998).
[4] M. Menon and D. Srivastava, Phys. Rev. Lett. **79**, 4453 (1997).
[5] F. L. Deepak, A. Govindaraj, and C. N. R. Rao, Chem. Phys. Lett. **345**, 5 (2001).
[6] L. P. Biró, S. D. Lazarescu, P. A. Thiry, A. Fonseca, J. B. Nagy, A. A. Lucas, and Ph. Lambin, Europhys. Lett. **50**, 494 (2000).
[7] L. P. Biró, R. Ehlich, Z. Osváth, A. Koós, Z. E. Horváth, J. Gyulai, and J. B. Nagy, Mater. Sci. Eng., C **19**, 3 (2002).
[8] L. P. Biró, G. I. Márk, A. A. Koós, J. B. Nagy, and Ph. Lambin, Phys. Rev. B **66**, 165404 (2002).
[9] Ph. Lambin, G. I. Márk, and L. P. Biró, Phys. Rev. B **67**, 205413-1 (2003).
[10] J. W. Park, J. Kim, J.-O. Lee, K. C. Kang, and J.-J. Kim, K.-H. Yoo, Appl. Phys. Lett. **80**, 133 (2002).
[11] P. M. Ajayan, V. Ravikumar, and J.-C. Charlier, Phys. Rev. Lett. **81**, 1437 (1998).
[12] F. Banhart, Rep. Prog. Phys. **62**, 1181 (1999).
[13] B. W. Smith and D. E. Luzzi, J. Appl. Phys. **90**, 3509 (2001).
[14] M. S. Raghuveer, P. G. Ganesan, J. D'Arcy-Gall, and G. Ramanath, Appl. Phys. Lett. **84**, 4484 (2004).
[15] M. Terrones, F. Banhart, N. Grobert, J.-C. Charlier, H. Terrones, and P. M. Ajayan, Phys. Rev. Lett. **89**, 075505-1 (2002).
[16] A. V. Krasheninnikov, K. Nordlund, and J. Keinonen, Phys. Rev. B **66**, 245403 (2002).
[17] H. Stahl, J. Appenzeller, R. Martel, Ph. Avouris, and B. Lengeler, Phys. Rev. Lett. **85**, 5186 (2000).
[18] A. Kis, G. Csányi, J.-P. Salvetat, Thien-Nga Lee, E. Couteau, A. J. Kulik, W. Benoit, J. Brugger, and L. Forró, Nat. Mater. **3**, 153 (2004).
[19] M. Terrones, H. Terrones, F. Banhart, J.-C. Charlier, and P. M. Ajayan, Science **288**, 1226 (2000).
[20] Y. Zhu, T. Yi, B. Zheng, and L. Cao, Appl. Surf. Sci. **137**, 83 (1999).
[21] M. Suzuki, K. Ishibashi, K. Toratani, D. Tsuya, and Y. Aoyagi, Appl. Phys. Lett. **81**, 2273 (2002).
[22] H. Lim, H. Jung, and S.-Ki. Joo, Microelectron. Eng. **69**, 81 (2003).
[23] B. Ni, R. Andrews, D. Jacques, D. Qian, M. B. J. Wijesundara, Y. Choi, L. Hanley, and S. B. Sinnott, J. Phys. Chem. B **105**, 12719 (2001).
[24] D. Srivastava, D. W. Brenner, J. D. Schall, K. D. Ausman, M. Yu, and R. S. Ruoff, J. Phys. Chem. B **103**, 4330 (1999).
[25] W. S. Yun, J. Kim, K. H. Park, J. S. Ha, Y. J. Ko, K. Park, S. K. Kim, Y. J. Doh, H. J. Lee, J. P. Salvetat, and L. Forró, J. Vac.

Sci. Technol. A **18**, 1329 (2000).
[26] A. V. Krasheninnikov, K. Nordlund, and J. Keinonen, Appl. Phys. Lett. **81**, 1101 (2002).
[27] A. V. Krasheninnikov and K. Nordlund, Nucl. Instrum. Methods Phys. Res. B **216**, 355 (2004).
[28] A. V. Krasheninnikov, Phys. Low-Dimens. Semicond. Struct. **11/12**, 1 (2000).
[29] A. V. Krasheninnikov, K. Nordlund, M. Sirviö, E. Salonen, and J. Keinonen, Phys. Rev. B **63**, 245405 (2001).
[30] A. V. Krasheninnikov and K. Nordlund, Phys. Solid State **44**, 470 (2002).
[31] V. Meunier and Ph. Lambin, Carbon **38**, 1729 (2000).
[32] D. Orlikowski, M. B. Nardelli, J. Bernholc, and C. Roland, Phys. Rev. B **61**, 14194 (2000).
[33] M. Ishigami, H. J. Choi, S. Aloni, S. G. Louie, M. L. Cohen, and A. Zettl, Phys. Rev. Lett. **93**, 196803-1 (2004).
[34] A. Hashimoto, K. Suenaga, A. Glotter, K. Urita, and S. Iijina, Nature (London) **430**, 870 (2004).
[35] L. Porte, M. Phaner, C. H. de Villeneuve, N. Moncoffre, and J. Tousset, Nucl. Instrum. Methods Phys. Res. B **44**, 116 (1989).
[36] J. R. Hahn and H. Kang, Phys. Rev. B **60**, 6007 (1999).
[37] A. V. Krasheninnikov, Solid State Commun. **118**, 361 (2001).
[38] M. T. Martínez, M. A. Callejas, A. M. Benito, M. Cochet, T. Seeger, A. Ansón, J. Schreiber, C. Gordon, C. Marhic, O. Chauvet, and W. K. Maser, Nanotechnology **14**, 691 (2003).
[39] D. Srivastava, M. Menon, C. Daraio, S. Jin, B. Sadanadan, and A. M. Rao, Phys. Rev. B **69**, 153414 (2004).
[40] A. H. Nevidomskyy, G. Csányi, and M. C. Payne, Phys. Rev. Lett. **91**, 105502 (2003).
[41] L. Porte, C. H. de Villeneuve, and M. Phaner, J. Vac. Sci. Technol. B **9**, 1064 (1991).
[42] L. P. Biró, J. Gyulai, Ph. Lambin, J. B. Nagy, S. Lazarescu, G. Márk, A. Fonseca, P. R. Surján, Zs. Szekeres, P. Thiry, and A. A. Lucas, Carbon **36**, 689 (1998).
[43] H. A. Mizes and J. S. Foster, Science **244**, 559 (1989).
[44] R. Saito, G. Dresselhaus, and M. Dresselhaus, *Physical Properties of Carbon Nanotubes* (Imperial College Press, London, 1998).
[45] G. M. Shedd and P. E. Russell, Surf. Sci. **266**, 259 (1992).
[46] E. L. Ivchenko and B. Spivak, Phys. Rev. B **66**, 155404 (2002).
[47] C. L. Kane and E. J. Mele, Phys. Rev. B **59**, R12759 (1999).